RSC Advances

ROYAL SOCIETY OF CHEMISTRY

www.rsc.org/advances

Adsorption of phosphate onto amine functionalized nano-sized magnetic polymer adsorbents: Mechanism and magnetic effect

Haoyu Shen[a]*, Zhejun Wang[a] , Ameng Zhou[a], Junliang Chen[a], Meiqin Hu[a], Xinyan Dong[a], Qinghua Xia[b]

[a] Ningbo Institute of Technology, Zhejiang University; Ningbo, 315100, China;

[b] Ministry-of-Education Key Laboratory for the Synthesis and Applications of Organic Functional Molecules, Hubei Collaborative Innovation Center for Advanced Organochemical Materials, Hubei University, Wuhan 430062, China

Abstract

A series of tetraethylenepentamine-functionalized core-shell structured nano magnetic Fe_3O_4 polymers (TEPA-Fe_3O_4-NMPs) with different amount of magnetic core were synthesized and characterized by XRD, EA, VSM, FTIR and XPS. Their applications as adsorbents for phosphate removal from aqueous solutions were studied. The adsorption mechanism and magnetic effect were intensively investigated. The adsorption processes of phosphate by TEPA-Fe_3O_4-NMPs were found highly pH dependent and related to the content of Fe_3O_4 magnetic core in the adsorbents. The optimized pH value was found at 3.0 for TEPA-Fe_3O_4-NMPs, while that of TEPA-Fe_3O_4-NMPs-0, which without Fe_3O_4 magnetic core, was found at 2.5. Kinetic studies showed that the adsorption of phosphate by TEPA-Fe_3O_4-NMPs followed pseudo-second-order model, with the adsorption rate constants, k_2, at 0.00274~0.0241 $g \cdot mg^{-1} \cdot min^{-1}$, suggesting chemisorption processes. Activation energies (E_a) for the phosphate removal varied with the content of Fe_3O_4 magnetic core, were found to be at 38.9~16.5 $kJ \cdot mol^{-1}$, indicating that the diffusion process might be the rate-controlled step. Thermodynamic studies suggested that the adsorption processes

*Corresponding author. Tel.: 86-574-88130130, E-mail address: hyshen@nit.zju.edu.cn (H. Y. Shen).

fit the Langmuir isotherms well with the optimized maximum adsorption capacities of phosphate onto the TEPA-Fe_3O_4-NMPs obtained when the content of Fe_3O_4 in TEPA-Fe_3O_4-NMPs was at 14.55 %. The Langmuir constants of apparent heat change, K_L, were found to be 0.0142~0.0461 $L \cdot mg^{-1}$, varied with the content of Fe_3O_4 magnetic core as well. FTIR and XPS analytic results of the adsorbents before and after phosphate adsorption suggested that phosphate had been successfully adsorbed onto TEPA-Fe_3O_4-NMPs *via* electrostatic attraction. The existing of the magnetic core might be favorable the mass transfer to accelerate the adsorption process.

Keywords: Tetraethylenepentamine-functionalized nano magnetic Fe_3O_4 polymers (TEPA-Fe_3O_4-NMPs); Phosphate; Magnetic effect; Adsorption; Mechanism

1. Introduction

Recently, nano magnetic polymers (NMPs) have been intensively studied, not only for scientific interest, but also for technological applications, such as magnetic fluids,[1] catalysis,[2] biotechnology/biomedicine,[3,4] contrast agents in magnetic resonance imaging (MRI), [5, 6] data storage, [7] and environmental remediation.[8-16]

However, bare magnetite nanoparticles are quite susceptible to air oxidation and are easily aggregated in aqueous systems. Although there have been many significant developments in the synthesis of magnetic nanoparticles, maintaining the stability of these particles for a long time without agglomeration or precipitation is an important issue. Recent research indicated that "core-shell" structured nano-magnetic polymers (NMPs) might be potential candidates as novel adsorbents. Functional polymers coating on the magnetic core enhanced the stability of nanodispersions by preventing their aggregation, moreover, the absorption properties can be tailored by suitable

functional groups. [10-15]

It is well known that trace amounts of phosphorus in water can lead to eutrophication problems. The phosphate concentration is regulated, and the maximum permissible is limited to 10 μg L^{-1} to escape eutrophication problems. [16, 17] With more and more strictly environmental regulations on the discharge of phosphorus and rising demands for clean water with extremely low levels of phosphorus, functionalized-magnetic nanoparticles, with enhanced adsorption rate, capacity, and selectivity, have gradually attracted researchers' great interest to be used as adsorbents for phosphorus removal.[18, 19] However, most researches about the magnetic core of NMPs were only focused on its intrinsic magnetic properties for facile solid-liquid separation under an applied magnetic field. Little attention was paid to the magnetic effects on the adsorption mechanism. Some results showed that magnetic composite materials presented higher adsorption capacities than a simple sum of the capacities of the non-interacting components, while some other results showed that there was no such a relationship.[13, 14, 20-22]

In the present work, TEPA-Fe_3O_4-NMPs with different Fe_3O_4 content were prepared to investigate their adsorption efficiencies towards phosphate. Batch adsorption tests were conducted to study the adsorption mechanism. The magnetic effect for phosphate removal was carried out by comparing the adsorption properties of the adsorbents with different magnetic Fe_3O_4 content. The results of kinetic and thermodynamic studies as well as XPS characterization suggested the Fe_3O_4 magnetic core in the adsorbents played a very important role during the adsorption process, not only on the arrangement of the amino groups on the surface of the adsorbents, but also on the species distribution of the phosphate in solution under different pH values.

2. Experimental

2.1 Chemicals

Glycidylmethacrylate (GMA), divinylbenzene (DVB), styrene (St) were sigma-aldrich products. Ferric chloride ($FeCl_3 \cdot 6H_2O$), ferrous sulphate ($FeSO_4 \cdot 7H_2O$), KH_2PO_4 was purchased from Sinopharm Chemical Reagent Co., Ltd (China). All the reagents were analytical grade. Distilled water was used to prepare all the solutions. 0.5 mol L^{-1} HNO_3 and 0.5 mol L^{-1} NaOH solutions were used for pH adjustment.

2.2 Adsorbents preparation

TEPA-Fe_3O_4-NMPs were synthesized according to our previous work[13] after a minor modification. Briefly, Fe_3O_4 particles were firstly encapsulated by oleic acids to obtain OA-M (oleic acids encapsulated magnetic Fe_3O_4); 2.0 g of polyglycol was dissolved into 200 mL hot water, followed by adding 0.5 mL DVB (0.0035 mol), 4 mL St (0.04 mol), and 8 mL GMA (0.052 mol). Then 1.0 g of OA-M was dispersed to the above system under ultrasonication. Finally, 1.0 g of benzoyl peroxide (BPO) dissolved in 20 mL ethanol was added dropwisely under vigorously stirring. The mixture was continuously reacted at 80 ^oC for 3 h, yielding epoxyl-Fe_3O_4-co-poly(DVB-St-GMA)s, named as eO-Fe_3O_4-NMPs. The final adsorbents (TEPA-Fe_3O_4-NMPs) were obtained by ring-opening reaction with TEPA. They were named as TEPA-Fe_3O_4-NMPs-0, TEPA-Fe_3O_4-NMPs-0.5, TEPA-Fe_3O_4-NMPs-1, TEPA-Fe_3O_4-NMPs-1.5, and TEPA-Fe_3O_4-NMPs-2, with the usage amount of Fe_3O_4 at 0, 0.5, 1, 1.5 and 2 g for preparation respectively. Overall preparation procedure was given in Fig S1 (Supplementary Information (SI)).

2.3 Characterization of TEPA-Fe_3O_4-NMPs

The structure and composition of the TEPA-Fe_3O_4-NMPs were investigated by a

vibrating sample magnetometer (VSM, Lake Shore 7410), elementary analysis (EA, Thermo Fisher Flash-1112), X-ray diffractometer analysis (XRD, Bruker D8 Advance), X-ray photoelectron spectroscopy (XPS, AXIS ULTRA ^{DLD}) and FTIR spectrometer (Thermo Nicolet NEXUS-470). Scanning electron microscopy (SEM) was performed using scanning electron microscopy (SEM, JSM-6700F) at an accelerating voltage of 5.0 kV. Sample dispersed at an appropriate concentration in ethanol was cast onto a silicon sheet at room temperature and sputter-coated with gold. Transmission electron microscopy (TEM) images were obtained on a Hitachi H-7650 transmission electron microscopy (TEM) (Hitachi, Japan) at an accelerating voltage of 75 kV.

2.4 Batch adsorption tests and analyses

The adsorption experiments were carried out in 100 mL stoppered flasks, each of which contained 40 mL of phosphate solution prepared with KH_2PO_4. A 0.02 g amount of adsorbents was added to each flask and shaken at 180 rpm in a thermostatic shaker. The concentration of phosphate was analyzed spectrophotometrically by the molybdenum blue method of National Standard of China (GB/T 6913-2008) at a wavelength of 690 nm, after a minor modification.[23] The amount of phosphate adsorbed per unit mass of adsorbents was evaluated as eq. (1) [13]:

$$q_e = \frac{(C_0 - C_e)V}{m} \quad (1)$$

Where q_e is the equilibrium adsorption capacity of phosphate ($mg \cdot g^{-1}$), C_0 is the initial concentration of phosphate ($mg \cdot L^{-1}$), C_e is the equilibrium concentration of phosphate ($mg \cdot L^{-1}$), V is the volume of the phosphate solution (mL), m is the adsorbent dosage

(mg), the same hereinafter.

To investigate the effect of pH, 40 mL of 100 mg·L^{-1} phosphate with pH ranging from 1.5 to 7.0 were mixed with 0.02 g of magnetic adsorbents for 3 h at 308 K, respectively. In the kinetic experiments, the TEPA-Fe_3O_4-NMPs were also investigated with contacting time ranging from 1~180 min at pH 3.0. The pseudo-first-order model (eq. (2)) and pseudo-second-order model (eq. (3))[24, 25] were used to fit the experimental data.

$$\log(q_e - q_t) = \log q_e - (\frac{k_1}{2.303})t \quad (2)$$

$$\frac{t}{q_t} = \frac{1}{k_2 q_e^2} + (\frac{1}{q_e})t \quad (3)$$

Where q_t is the adsorption capacity at time t (mg·g^{-1}), k_1 (min^{-1}), k_2 (g·mg^{-1}·min^{-1}) are the adsorption rate constants.

The adsorption isotherm studies were investigated with phosphate initial concentrations ranging from 50 to 700 mg·L^{-1}, under pH of 3.0 and at 308K for 3 h. Two adsorption isotherms, Langmuir model (eq. (4))[26] and Freundlich model (eq. (5))[27], were applied to analyze the adsorption data.

$$\frac{C_e}{q_e} = \frac{1}{K_L q_m} + \frac{C_e}{q_m} \quad (4)$$

$$\log q_e = \log K_F + (1/n)\log C_e \quad (5)$$

Where q_m and K_L are the Langmuir constants related to the maximum adsorption capacity and apparent heat change, respectively, while K_F and n are the constants of Freudlich model.

3. Results and discussion

3.1 Characterization of TEPA-Fe_3O_4-NMPs

The microspheres of TEPA-Fe_3O_4-NMPs with the usage amount of Fe_3O_4 were similar. The SEM and TEM images of TEPA-Fe_3O_4-NMPs-1 were shown in Fig. S2(a) and (b), respectively. It revealed that the TEPA-Fe_3O_4-NMPs particles were multidispersed with an average diameter of around 300 nm.

3.1.1 XRD analyses

Fig. 1 showed the XRD analysis of TEPA-Fe_3O_4-NMPs as well as the bare Fe_3O_4. It indicated that TEPA-Fe_3O_4-NMPs had retained the spinel structure of Fe_3O_4, in which the identical peaks for Fe_3O_4 located at 30.1°, 35.5°, 43.1°, 53.4°, 57.0° and 62.6°, corresponding to their indices (220), (311), (400), (422), (511) and (400)[28] appeared. The intensity of diffraction peaks became slightly stronger with the content of Fe_3O_4 increased.

<Insert Fig. 1>

3.1.2 Fe_3O_4 content, Elementary analysis (EA) and VSM analysis

The Fe_3O_4 content of each TEPA-Fe_3O_4-NMPs was calculated from the amount of leached Fe, which was measured by using a spectrophotometer (722, Shanghai, China) according to the standard colorimetric method[29] after digesting TEPA-Fe_3O_4-NMPs in 12 $mol \cdot L^{-1}$ HCl solution. The results were shown in Table 1. It indicated that the Fe_3O_4 content of the TEPA-Fe_3O_4-NMPs increased from 13.49% to 19.24%, with the usage amount of Fe_3O_4 increasing from 0.5 g to 2 g, during the synthesis process.

The elementary analysis results of the nitrogen contents in TEPA-Fe_3O_4-NMPs were listed in Table 1 as well. It showed that the nitrogen contents decreased from 5.00 $mmol \cdot g^{-1}$ for TEPA-Fe_3O_4-NMPs-0 to 3.55 $mmol \cdot g^{-1}$ for TEPA-Fe_3O_4-NMPs-2.

The vibrating sample magnetometer (VSM) was applied to test the magnetic properties of TEPA-Fe_3O_4-NMPs as shown in Fig. 2. The saturation moments of the four TEPA-Fe_3O_4-NMPs were found to be 9.77, 10.59, 12.39, 12.78 emu·g^{-1} (listed in Table 1), respectively. Since the polymer shell was diamagnetism, it was reasonable that the ratio of paramagnetic composition reduced, which led to lower saturation moments than that of the bare Fe_3O_4, (73.98 emu·g^{-1}, Fig. 2(e), insert). The magnetism of the TEPA-Fe_3O_4-NMPs enhanced with the content of Fe_3O_4 increased.

<Insert Table 1>

<Insert Fig. 2>

3.1.3 XPS analyses

XPS spectra of on TEPA-Fe_3O_4-NMPs were tested. Typical spectra of TEPA-Fe_3O_4-NMPs-1 for both survey and high-resolution scans before and after adsorption were shown in Fig. 3. For those with Fe_3O_4 cores, the ratio of Fe(II)/Fe(III) on the surface of the TEPA-Fe_3O_4-NMPs was ~0.48. The deconvolved values were very close to those of magnetite (Fe_3O_4) reported in literatures[30-32]. Atomic concentrations of the key elements in TEPA-Fe_3O_4-NMPs were summerized in Table 2. It indicated that although with the increasing of the total content of Fe_3O_4 in the TEPA-Fe_3O_4-NMPs from 13.49% to 19.24%, as discussed above, the concentration of the Fe element on their surfaces did not vary much (0.4%~0.54%). On the contrary, the concentration of the N element on their surfaces increased from 4.53% to 8.53%, with the usage amount of Fe_3O_4 increasing from 0.5 g to 2 g, even though the total contents of the nitrogen decreased as founded in elemental analysis. Atomic concentration of nitrogen on the surface of the TEPA-Fe_3O_4-NMPs-0 was found only

to be 4.54%, which was the lowest one in the studied adsorbents. Since only the number of electrons that escape from the top 1 to 10 nm of materials can be analyzed by XPS, this result implied that the existing of the magnetic core might be favorable the arrangement of the amino groups on the surface of the TEPA-Fe_3O_4-NMPs, leading fewer amino groups (-NH- and -NH_2) immersed in the polymer matrix.

<Insert Fig. 3>

<Insert Table 2>

3.2 Adsorption properties

3.2.1 Effect of pH

The effect of pH on phosphate adsorption over the range of 1.5 to 7.0 was investigated. The results demonstrated that the pH values of the solutions had a significant effect on the adsorption properties of TEPA-Fe_3O_4-NMPs to phosphate (Fig. 4.). The pH dependency might be related both to the intrinsic structure property of the TEPA-Fe_3O_4-NMPs and the species of phosphate. Under acidic conditions, amine groups were easier to be protonated (-NH_3^+), as shown in Eq. (6). Phosphate existed in the forms of H_3PO_4, $H_2PO_4^-$, HPO_4^{2-} and PO_4^{3-} (shown in Fig. 5), depending on the solution pH (pK_1 = 2.15, pK_2 = 7.20, and pK_3 = 12.33).[16, 19] With an increase of pH, the TEPA-Fe_3O_4-NMPs surface carried positive charge, and thus would more significantly attract the negatively charged monovalent $H_2PO_4^-$ ions in solution, which indicated that the physicochemical adsorption due to electrostatic attraction was the predominant process of phosphate removal, as described by Eq. (7). When the pH of the solution increased, the surface became negatively charged, consequently, unfavorable to the phosphate for electrostatic repulsion.

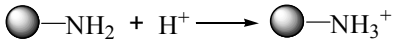

(6)

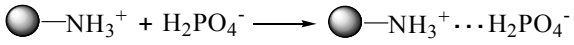

(7)

Interestingly, the optimized pH value was found at 3.0 for TEPA-Fe_3O_4-NMPs, while that of TEPA-Fe_3O_4-NMPs-0, which without Fe_3O_4 magnetic core, was at 2.5 (Fig. 4.). Based on the experimental data of the total concentration of phosphate, we run Visual MINTEQ 3, which is widely used in recent years to simulate equilibria and speciation of inorganic solutes in aqueous solution. [33, 34] The speciation of phosphate under various pH was obtained, as shown in Fig S3, the highest fraction of $H_2PO_4^-$ occurred at pH=2.5 for TEPA-Fe_3O_4-NMPs-0, while at pH=3.0 for TEPA-Fe_3O_4-NMPs-0.5, TEPA-Fe_3O_4-NMPs-1.0, TEPA-Fe_3O_4-NMPs-1.5, and TEPA-Fe_3O_4-NMPs-2.0, which were consistent with the experimental results. The results inferred that the existing of magnetic core might have some effect on species distribution in solution. This could be further explained by the results of the zeta potential of the TEPA-Fe_3O_4-NMPs. As shown in Fig. S4, The pH of zero point of charge (pH_{zpc}) was observed at pH 2.48, 2.98, 3.02, 2.99, 3.02, 3.04, for TEPA-Fe_3O_4-NMPs-0, TEPA-Fe_3O_4-NMPs-0.5, TEPA-Fe_3O_4-NMPs-1.0, TEPA-Fe_3O_4-NMPs-1.5 and TEPA-Fe_3O_4-NMPs-2.0, respectively. Positive zeta potential was found to be at pH of 2.48 for TEPA-Fe_3O_4-NMPs-0, while 2.98-3.05 for other TEPA-Fe_3O_4-NMPs, indicating that the particles were positive charged. Thus, electrostatic interaction would be favorable for anionic ions ($H_2PO_4^-$) adsorption. Negative zeta potential of TEPA-Fe_3O_4-NMPs was found at pH above the pH_{ZPC}. The repulsion between the negatively charged surface of the adsorbent and the anions, *i.e.*, $H_2PO_4^-$, $H_2PO_4^{2-}$, PO_4^{3-}, *etc*, resulting in low adsorption capacities. Although the saturation moments TEPA-Fe_3O_4-NMPs are quite small (9.77~12.78 emu·g^{-1}), their magnetic effects on the species distribution of the phosphate in solution under

different pH values are not negligible.

<Insert Fig. 4>

<Insert Fig. 5>

3.2.2 Adsorption kinetic studies

Kinetic studies were carried out and the experimental results were presented in Fig. 6. As shown in Fig. 6(a), compared to the TEPA-Fe_3O_4-NMPs with Fe_3O_4 cores, 90 mins were needed for the TEPA-Fe_3O_4-NMPs-0 to reach adsorption equilibrium, while less than 10 mins for TEPA-Fe_3O_4-NMPs containing a certain amount of Fe_3O_4 were needed. This revealed that the presence of Fe_3O_4 in adsorbents could effectively shorten the equilibrium time. Besides, the kinetic curve of TEPA-Fe_3O_4-NMPs-0 could be divided into three portions, which could be described by intraparticle diffusion model (shown in Fig. 6(b)) and indicated that the intra-particle process[14] might be one of the rate-limiting steps for phosphate removal by TEPA-Fe_3O_4-NMPs-0. Unlike the TEPA-Fe_3O_4-NMPs-0, the kinetic curves of TEPA-Fe_3O_4-NMPs containing a certain amount of Fe_3O_4, could only be divided into only two portions (Fig. 6(b)), thus, the intra-particle process might not be involved in the rate-limiting steps. The probable reason was that, as for TEPA-Fe_3O_4-NMPs-0, without magnetic core, a large part of amino groups might be embedded in the polymer matrices, as found in XPS as we discussed above, phosphate ions migrating to contact with those active groups needed longer time to reach equilibrium. The existence of the Fe_3O_4 cores in the TEPA-Fe_3O_4-NMPs might eliminate intra-particle diffusion.

Pseudo-first-order and pseudo-second-order models were used to describe the

adsorption kinetic data. The correlation coefficient values indicated a better fit of the pseudo-second-order model with the experimental data compared to the pseudo-first-order for all the five adsorbents (Table 3). The calculated q_e values were in agreement with the theoretical ones, and the plots showed good linearity with R^2 above 0.99. Therefore, the adsorption behaviors followed the pseudo-second-order model, suggesting a chemisorption process. [25]

Adsorption kinetic at different temperatures (25 ^oC~45 ^oC) was carried out. The Arhenius equation was applied to investigate the E_a for the adsorption process.

$$k = Ae^{-E_a/RT} \quad (8)$$

k refers to the pseudo-second-order rate constant ($g \cdot mg^{-1} \cdot min^{-1}$); E_a is the activation energy of phosphate adsorption ($kJ \cdot mol^{-1}$); A is the pre-exponential factor (frequency factor); R is the gas constant (8.314 $J \cdot mol^{-1} \cdot K^{-1}$); T is the adsorption temperature (K).

From the linear relationships between ln$k$ and 1/T (Fig. 6(c)), for the process of adsorbing phosphate onto the TEPA-Fe_3O_4-NMPs, E_a was found to be 38.9, 25.2, 22.1, 18.9, 16.5 $kJ \cdot mol^{-1}$ for TEPA-Fe_3O_4-NMPs-0, TEPA-Fe_3O_4-NMPs-0.5, TEPA-Fe_3O_4-NMPs-1, TEPA-Fe_3O_4-NMPs-1.5, and TEPA-Fe_3O_4-NMPs-2, respectively (all were less than 42 $kJ \cdot mol^{-1}$), indicating that diffusion process was the rate-controlled step.[35]

Interestingly, except TEPA-Fe_3O_4-NMP-0, a fine linear relationship between k_2 and the saturation moments of the TEPA-Fe_3O_4-NMPs, was observed, shown in Fig. 6 (d). The relationship between the activation energy changes ($\triangle E_a = E_{a,\ \text{TEPA-Fe3O4-NMPs}} - E_{a,\ \text{TEPA-Fe3O4-NMPs-0}}$) and the saturation moments was further observed, shown in Fig. 6 (d, insert), it was found that the $\triangle E_a$ linearly decreased with the increasing of the saturation moments of the TEPA-Fe_3O_4-NMPs, was observed, shown in Fig. 6 (d). This phenomenon inferred that the higher the saturation moments of the

TEPA-Fe_3O_4-NMPs was, the faster the adsorption process achieved. The existing of the magnetic core might be favorable the mass transfer to accelerate the adsorption process. On the contrary, k_2 decreased with the increase of nitrogen contents of the TEPA-Fe_3O_4-NMPs linearly, including TEPA-Fe_3O_4-NMP-0, shown in Fig. 6 (e). Although the total functional groups of amine (-NH- and -NH_2) increased as the nitrogen contents increased, some of the active sites might be immersed in the polymer matrix of the TEPA-Fe_3O_4-NMPs, some transfer barriers occurred and the equilibrium time increased accordingly, which was consistent with the findings of the none-magnetic amino-functional polymers.[19]

<Insert Fig. 6>

<Insert Table 3>

3.2.3 Thermodynamic studies

The thermodynamic parameters, *i.e.*, standard free energy change ($\triangle G^{\theta}$), enthalpy change ($\triangle H^{\theta}$), and entropy change ($\triangle S^{\theta}$), were estimated to evaluate the feasibility and exothermic nature of the adsorption process. The Gibb's free energy change of the process is related to equilibrium constant by eq. (9):

$$\Delta G^{\theta} = -RT \ln K_D \tag{9}$$

where K_D is the distribution coefficient, which is defined as eq. (10),

$$K_D = \frac{q_e}{C_e} = \frac{\text{Amount of phosphate adsorbed on TEPA-Fe}_3\text{O}_4\text{-NMPs}}{\text{Amount of phosphate in solution}} \times \frac{V}{m} \tag{10}$$

According to thermodynamics, the Gibb's free energy change ($\triangle G^{\theta}$) is also related to the enthalpy change ($\triangle H^{\theta}$) and entropy change ($\triangle S^{\theta}$) at constant temperature by eq. (11):

$$\Delta G^{\theta} = \Delta H^{\theta} - T\Delta S^{\theta} \quad (11)$$

Thus,
$$\ln K_D = \frac{\Delta S^{\theta}}{R} - \frac{\Delta H^{\theta}}{RT} \quad (12)$$

The values of enthalpy change ($\triangle H^{\theta}$) and entropy change ($\triangle S^{\theta}$) were calculated from the slope and intercept of the plot of $\ln K_D$ *vs* ($1/T$). The results of the five adsorbents were shown in Fig. 7. These thermodynamic parameters were given in Table 4. As listed in Table 4, the enthalpy changes ($\triangle H^{\theta}$) for the five adsorbents were found to be at 16.54 ~ 7.86 kJ·mol^{-1}, which indicated that the adsorption was endothermic. The entropy changes ($\triangle S^{\theta}$) were in range of 56.78 ~ 27.60 J·mol^{-1}·K^{-1}. The values of $\triangle G^{\theta}$ were all negative for the TEPA-Fe_3O_4-NMPs with different amount of magnetic nuclei, implying the spontaneous nature of the adsorption process.

<Insert Fig. 7>

<Insert Table 4>

3.2.4 Adsorption capacities

The adsorption capacities of phosphate were investigated for the adsorbents containing different usage amount of magnetic core (Fe_3O_4) (Fig. 8). The represented parameters using Langmuir and Freundlich adsorption models indicated that the Langmuir model could effectively describe the adsorption data with $R^2 > 0.99$ (Table 5), suggesting a better fit of the Langmuir isotherm rather than Freundlich isotherm, which suggested a monolayer adsorption.

As shown in Fig. 8(a) and Table 5, the usage amount of Fe_3O_4 could obviously

affect the adsorption efficiency. The maximum adsorption capacities of phosphate onto the TEPA-Fe_3O_4-NMPs increased from 77.52 $mg \cdot g^{-1}$ to 102.04 $mg \cdot g^{-1}$ with an increase in the usage amount of Fe_3O_4 for TEPA-Fe_3O_4-NMPs preparation from 0 to 1.0 g, then decreased from 104.04 $mg \cdot g^{-1}$ to 92.59 $mg \cdot g^{-1}$ with increasing the usage amount of Fe_3O_4 from 1.0 to 2.0 g. Similarly, although TEPA-Fe_3O_4-NMPs-0 contained the largest amount of amine (-NH- and $-NH_2$) groups (5.0 $mmol \cdot g^{-1}$), its adsorption capacity (77.52 $mg \cdot g^{-1}$) was the lowest among the present studied adsorbents. TEPA-Fe_3O_4-NMPs-2, with the largest amount of Fe_3O_4, had the second lowest adsorption capacity (92.59 $mg \cdot g^{-1}$). These results indicated that the adsorption capacity would not be simply related to the amount of amine (-NH- and $-NH_2$) groups on the adsorbents.[19] The content of Fe_3O_4 in the adsorbents may also play an important role in the removal of phosphate. The adsorption capacity of phosphate may be an integrated result of both the amount of amine (-NH- and $-NH_2$) groups and Fe_3O_4 content in the magnetic adsorbents since neither of them fully reflected the present finding. TEPA-Fe_3O_4-NMPs-1, with the highest adsorption capacity for phosphate removal, may have an appropriate ratio of amine (-NH- and $-NH_2$) groups and Fe_3O_4 content. We further tested the adsorption capacity of bare Fe_3O_4 to phosphate, which was found to be 17.06 $mg \cdot g^{-1}$. The results showed that the sum of adsorption capacities of bare Fe_3O_4 and TEPA-Fe_3O_4-NMPs-0 was found to be 94.58 $mg \cdot g^{-1}$ (Fig. 8(b)). It clearly implied that the adsorption capacity of TEPA-Fe_3O_4-NMPs to phosphate was not a simple sum of the two isolated components (Fe_3O_4 core and polymeric layer). There might be some cooperative interactions between them. From our present investigation, the equilibrium constant K_L was found to increase from 0.0304 to 0.0747 $L \cdot mg^{-1}$ with the usage amount of Fe_3O_4 increasing from 0.5 to 2.0 g for synthesis, as shown in Table 5. The results

implied that the presence of Fe_3O_4 in the magnetic adsorbents would be favorable for the achievement of maximum adsorption capacity. The more Fe_3O_4 contained in the adsorbents, the more significant the effect was.

<Insert Fig. 8>

<Insert Table 5>

3.3 Adsorption mechanism

To further investigate the mechanism of phosphate adsorbing onto TEPA-Fe_3O_4-NMPs, VSM, FTIR and XPS techniques were applied to distinguish the difference of before and after phosphate loading onto TEPA-Fe_3O_4-NMPs-1.

The magnetic performance comparison of TEPA-Fe_3O_4-NMPs-1 before and after loading phosphate ions was carried out by VSM analysis (Fig. 9). As shown in Fig. 9, the saturation moment reduced from 10.59 emu·g^{-1} to 9.58 emu·g^{-1} after phosphate ions adsorption. Since phosphate ion was diamagnetism, it was reasonable that the ratio of paramagnetic composition reduced for the post-adsorbed magnetic adsorbent.

<Insert Fig. 9>

The IR spectra of TEPA-Fe_3O_4-NMPs-1 before (a) and after adsorption of phosphate (b) were showed in Fig. 10. In Fig. 10 (a), the broad peak appeared at ~3360 cm^{-1} and ~1573 cm^{-1} can be assigned to be the stretching and bending vibrations of the -NH and -NH_2 groups. While after adsorption, in Fig. 10 (b), the characteristic bands at ~1573 cm^{-1} disappeared along with the appearance of the bands at ~1630 cm^{-1}, which may be attributed to the interaction between amino groups and the phosphate groups, subsequently weakened the N-H bonding and resulted in a large

shift (~80 cm^{-1}). The characteristic peaks of the phosphate groups at 543 cm^{-1} were also observed in Fig. 10 (b), corresponding to the -P-O and -O-P-O groups, respectively.[38] It indicated that the phosphate groups adsorbed successfully onto the TEPA-Fe_3O_4-NMPs-1.

<Insert Fig. 10>

XPS spectra of both survey and high-resolution scans for the key elements on TEPA-Fe_3O_4-NMPs-1 surfaces before and after adsorption (Fig. 3) were furtherly investigated to gain more insights on the interaction mechanism. From the survey spectra (Fig. 3(a)), and the high-resolution XPS spectra (Fig. 3(b)), the new peak, appeared at 131.8 eV, which can be assigned to P2p, clearly confirmed the successful adsorption of phosphate.[39] As shown in Fig. 3(c), after adsorption, the peaks of N1s at 396.8 eV shifted to higher binding energies (~398.8 eV) with a broader band range. The shift of the N1s peaks could be attributed to protonated amine groups ($–NH_3^+$) and the further formation of $–NH_3^+\cdots H_2PO_4^-$.[40] The effects from electrostatic attraction would make the outer-shell electron density of N atoms reduced, which caused the nuclear charge on the inner electron shielding effect to be weakened. The inner electron binding energy of N1s increased, so the peaks of N1s in XPS spectra shifted to higher binding energies.[13] Similar phenomena were observed in the XPS spectra of O1s (Fig. 3 (d)), peaks of O1s appeared at ~530 eV and ~527.9 eV, assigned to C-O-C and C-OH groups, broadening with a slight shift of binding energies. In the XPS spectra of C1s (Fig. 3 (e)), the carbon atoms can be found in two chemically different positions, leading to two differing C1s binding energies: C-O-C (~282.9 eV) and C-O-C or C-OH (~286.5 eV). After adsorption, the peaks at ~282.9

eV shifted to higher binding energies (~283.9 eV) with a broader band range, while the peaks at ~286.5 eV disappeared, which may attribute to the involvement of the –OH groups in the adsorption phosphate.

Changes in atomic concentration of the key elements after the adsorption were summerized in Table 2. After adsorption of phosphate, the atomic concentration of the P element on their surfaces increased from 0.58% to 1.76%, with the usage amount of Fe_3O_4 increasing from 0.5 g to 2 g, which was consistent with that of nitrogen element. The presence of Fe_3O_4 in the magnetic adsorbents would be favorable to the achievement of maximum adsorption capacity with less equilibrium time.

Presumed adsorption mechanism was shown in Scheme 1. Under acidic conditions, the functional amino groups were first protonated. $H_2PO_4^-$ ions adsorbed onto the TEPA-Fe_3O_4-NMPs via electrostatic attraction as described above (Eq (6) and (7)). Since atomic concentration of nitrogen on the surfaces of TEPA-Fe_3O_4-NMPs increased from 4.53% to 8.53%, with the usage amount of Fe_3O_4 increasing from 0 g to 2 g, as found in XPS, the existing of the magnetic core might be favorable the arrangement of the amino groups on the surface of the TEPA-Fe_3O_4-NMPs, leading fewer amino groups (-NH- and -NH_2) immersed in the polymer matrix, as shown in Scheme 1 (a) and (b), thus comparing to TEPA-Fe_3O_4-NMPs-0, less time needed for other TEPA-Fe_3O_4-NMPs for phosphate migrating to active groups to reach equilibrium, shown in Scheme 1 (c) and (d).

<Insert Scheme 1>

4. Conclusions

The removal of phosphate from aqueous solution by TEPA-Fe_3O_4-NMPs was

studied. The effect of parameters, such as solution pH, contact time, solution temperature, Fe_3O_4 amount on the surface and in adsorbents, were investigated. An intensive investigation on the adsorption mechanism and the magnetic effect was studied. The results suggested that the adsorption processes were highly pH dependent. The kinetic studies revealed that the adsorption of phosphate onto TEPA-Fe_3O_4-NMPs followed pseudo-second-order model. Thermodynamic studies suggested that the adsorption processes of phosphate onto the TEPA-Fe_3O_4-NMPs were endothermic and entropy favored in nature. The content of Fe_3O_4 in the adsorbents could obviously affect the adsorption efficiencies. TEPA-Fe_3O_4-NMPs-1, with the highest adsorption capacity for phosphate removal at 102.04 $mg \cdot g^{-1}$, may had an appropriate ratio of amino groups and Fe_3O_4 content. The adsorption capacity of phosphate by TEPA-Fe_3O_4-NMPs may be an integrated result of both the amount of amino groups and Fe_3O_4 content in the magnetic adsorbents. The existing of magnetic core in the TEPA-Fe_3O_4-NMPs was found to be able to eliminate the intra-particle diffusion, but accelerate and strengthen the adsorption equilibrium processes, with larger equilibrium constant K_L and pseudo-second-order rate constant k_2. The results from XPS analyses indicated that the existing of the magnetic core might be favorable the arrangement of the amino groups on the surface of the TEPA-Fe_3O_4-NMPs, which may be favorable the mass transfer to accelerate the adsorption process.

Acknowledgments

We would like to thank the National Natural Science Foundation of Zhejiang Province (LY14B04003), the National Natural Science Foundation of Ningbo (2014A610092), the National College Students' innovation and entrepreneurship training program (201413022011), the Xinmiao Students' innovation training program

of Zhejiang Province (2014R401190) for the financial support.

References

1 P. Mahato, S. Saha, P. Das, H. Agarwallad and A. Das, *RSC Adv.*, 2014, **4**, 36140.

2 N. Singh and K. Balasubramanian, *RSC Adv.*, 2014, **4**, 27691.

3 A. H. Lu, E. L. Salabas and F. Schuth. *Angew. Chem. Int. Ed.*, 2007, **46**, 1222.

4 J. Kim, J. E. Lee, J. Lee, J. H. Yu, B. C. Kim, K. An, Y. Hwang, C. H. Shin, J. G. Park, J. Kim, and T. Hyeon. *J. Am. Chem. Soc.*, 2006, **128**, 688.

5 S. T. Xing, D. Y. Zhao, W. J. Yang, Z. C. Ma, Y. S. Wu, Y. Z. Gao, W. R. Chen and J. Han. *J. Mater. Chem. A*, 2013, **1**, 1694.

6 M. C. K. Wiltshire, J. B. Pendry, I. R. Young, D. J. Larkman, D. J. Gilderdale and J. V. Hajnal. *Science*, 2001, **291**, 849.

7 Y. W. Jun, Y. M. Huh, J. S. Choi, J. H. Lee, H. T. Song, S. Kim, S. Yoon, K. S. Kim, J. S. Shin, J. S. Suh and J. Cheon. *J. Am. Chem. Soc.*, 2005, **127**, 5732.

8 C. Paul, Inkjet printing for materials and devices, *Chem. Mater.* 2001, **13**, 3299.

9 S A. Ghosal, J. Shah, R. K. Kotnala and S. Ahmad. *J. Mater. Chem. A*, 2013, **1**, 12868.

10 R. D. Ambashta, and S. Mika. *J. Hazard. Mater.*, 2010, **180**, 38.

11 Y. G. Zhao, H. Y. Shen, S. D. Pan, and M. Q. Hu. *J. Hazard. Mater.*, 2010, **182**, 295.

12 H. Y. Shen, S. D. Pan, Y. Zhang, X. L. Huang, and H. X. Gong. *Chem. Eng. J.*, 2012, **183**, 180.

13 H. Y. Shen, J. L. Chen, H. F. Dai, L. B. Wang, M. Q. Hu and Q. H. Xia. *Ind. Eng. Chem. Res.*, 2013, **52**, 12723.

14 S. D. Pan, Y. Zhang, H. Y. Shen and M. Q. Hu. *Chem. Eng. J*., 2012, **210**, 564.

15 Y. G. Zhao, X. H. Chen, S. D. Pan, H. Zhu, H. Y. Shen and M. C. Jin. *J. Mater. Chem. A.*, 2013, **1**, 11648.

16 Y. Zhang, S. D. Pan, H. Y. Shen and M. Q. Hu. *Anal. Sci.*, 2012, **28**, 887.

17 L. A. Rodrigues and M. L. C. P. da Silva. *Desalination*, 2010, **263**, 29.

18 F. Özmen, P. A. Kavakli and O. Güven. *J. Appl. Polym. Sci.*, 2011, **119**, 613.

19 Y. Zhang, X. Q. Xi, S. N. Xu, J. C. Zhou, J. J. Zhou, Q. H. Xu and H. Y. Shen. *Acta Chim. Sin.*, 2012, **70**, 1839.

20 M. M. Amin, B. Bina, A. M. S. Majd, and H. Pourzamani. *Front. Environ. Sci. Engineer.*, 2014, **8**, 345.

21 F. Aboufazeli, H. R. L. Z. Zhad, O. Sadeghi, M. Karimi and E. Najafi. *Food. Chem.*, 2013, **141**, 3459.

22 M. E. Mahmoud, M. S. Abdelwahab and E. M. Fathallah. *Chem. Eng. J.*, 2013, **223**, 318.

23 Ministry of Health, and Standardization Administration, the People's Republic of China, GB/T 6913-2008 Standard examination methods for phosphate in boiler-used water and cooling water, 2008.

24 J. X. Lin and L. Wang. *Front. Environ. Sci. Engineer. Chi.*, 2009, **3**, 320.

25 Y. S. Ho. *J. Hazard. Mater.*, 2006, **136**, 681.

26 Y. Chen, B. Pan, H. Li, W. Zhang, L. Lv and J. Wu. *Environ. Sci. Technol.*, 2010, **44**, 3508.

27 M. Owlad, M. K. Aroua and W. M. A. W. Daud. *Bioresour. Technol.*, 2010, **101**,

5098.

28 W. S. Lu, Y. H. Shen, A. J. Xie, X. Z. Zhang and W. G. Chang. *J. Phys. Chem. C*, 2010, **114**, 4846.

29 B. X. Cai and Y. W. Chen. Basical Chemistry Experiments, Science Press, Beijing, China, 2001.

30 X. F. Sun, Y. Ma, X. W. Liu, S. G. Wang, B. Y. Gao and X. M. Li. *Water Res.*, 2010, **44**, 2517.

31 S. R. Chowdhury, E. K. Yanful and A. R. Pratt. *J. Hazard. Mater.*, 2012, **235-236**, 246.

32 D. K. Park, Y. S. Yun and J. M. Park. *J. Colloid Interface Sci.*, 2008, **317**, 54.

33 E. Nehrenheim and J. P. Gustafsson. *Bioresource Techn.*, 2008, **99**, 1571.

34 E. Vasyukova, O. S. Pokrovsky, J. Viers and B. Dupre. *Appl. Geochem*., 2012, **27**, 1226.

35 E. I. El-Shafey. *J. Hazard. Mater.*, 2010, **175**, 319.

36 J. W. Choi, Y. S. Choi, S. W. Hong, D. J. Kim and S. H. Lee. *Water Environ. Res.*, 2012, **84**, 596.

37 R. Saad, K. Belkacemi and S. Hamoudi. *J. Colloid. Interface. Sci.*, 2007, **311**, 375.

38 T. S. Anirudhan and P. Senan. *Chem. Ecol.*, 2011, **27**, 147.

39 H. B. Ma, J. Li, H. Chen, G. Z. Zuo, Y. Yu, T. H. Ren and Y. D. Zhao. *Tribol. Int.*, 2009, **42**, 940.

40 Z. Nazarpoor, S. Ma, P. T. Fanson, O. S. Alexeev and M. D. Amiridis. *Polym. Degrad. Stab.*, 2012, **97**, 439.

Figures and Scheme Captions

Fig. 1 XRD spectra of (a) Fe_3O_4; (b) TEPA-Fe_3O_4-NMPs-0.5; (c) TEPA-Fe_3O_4-NMPs-1; (d) TEPA-Fe_3O_4-NMPs-1.5; (e) TEPA-Fe_3O_4-NMPs-2;

Fig. 2 VSM spectra of (a) TEPA-Fe_3O_4-NMPs-0.5; (b) TEPA-Fe_3O_4-NMPs-1; (c) TEPA-Fe_3O_4-NMPs-1.5; (d) TEPA-Fe_3O_4-NMPs-2; (e) bare Fe_3O_4 (insert)

Fig. 3 XPS spectra of: (a) survey scan, and high-resolution scan of: (b) P2p；(c) N1s；(d) O1s；(e) C1s；(f) Fe2p;

Fig. 4 Effect of pH on the removal of phosphate by different adsorbents;

Fig. 5 Distribution diagrams of phosphate species;

Fig. 6 Kinetic results for phosphate adsorption: (a) for different adsorbents; (b) Intraparticle diffusion model of phosphate adsorption onto TEPA-Fe_3O_4-NMPs with different usage amounts of magnetic core; (c) plot of ln$k$ *vs* 1/T; (d) Relationship between k_2 and $\triangle E_a$ (insert) and the saturation moments of the TEPA-Fe_3O_4-NMPs; (e) Relationship between k_2 and the nitrogen contents of the TEPA-Fe_3O_4-NMPs;

Fig. 7 Thermodynamitic results of adsorption of phosphate onto TEPA-Fe_3O_4-NMPs;

Fig. 8 Adsorption isotherm of phosphate onto different adsorbents;

Fig. 9 VSM analysis of: (a) TEPA-Fe_3O_4-NMPs-1; (b) TEPA- Fe_3O_4-NMPs-1-P;

Fig. 10 FTIR analysis of: (a) TEPA- Fe_3O_4-NMPs-1; (b) TEPA-Fe_3O_4-NMPs-1-P;

Scheme 1 Presumed adsorption mechanism

Tables

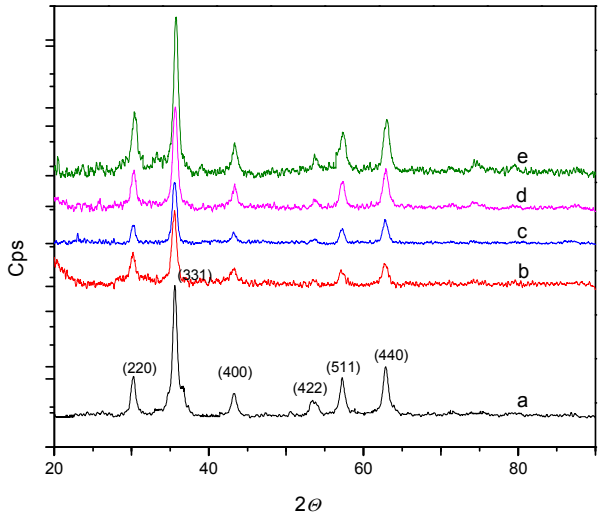

Fig. 1 XRD spectra of (a) Fe_3O_4; (b) TEPA-Fe_3O_4-NMPs-0.5; (c) TEPA-Fe_3O_4-NMPs-1; (d) TEPA-Fe_3O_4-NMPs-1.5; (e) TEPA-Fe_3O_4-NMPs-2

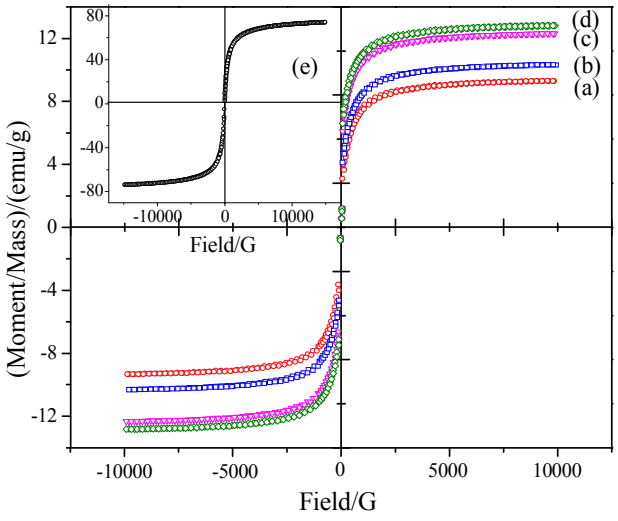

Fig. 2 VSM spectra of (a) TEPA-Fe_3O_4-NMPs-0.5; (b) TEPA-Fe_3O_4-NMPs-1; (c) TEPA-Fe_3O_4-NMPs-1.5; (d) TEPA-Fe_3O_4-NMPs-2; (e) bare Fe_3O_4 (insert)

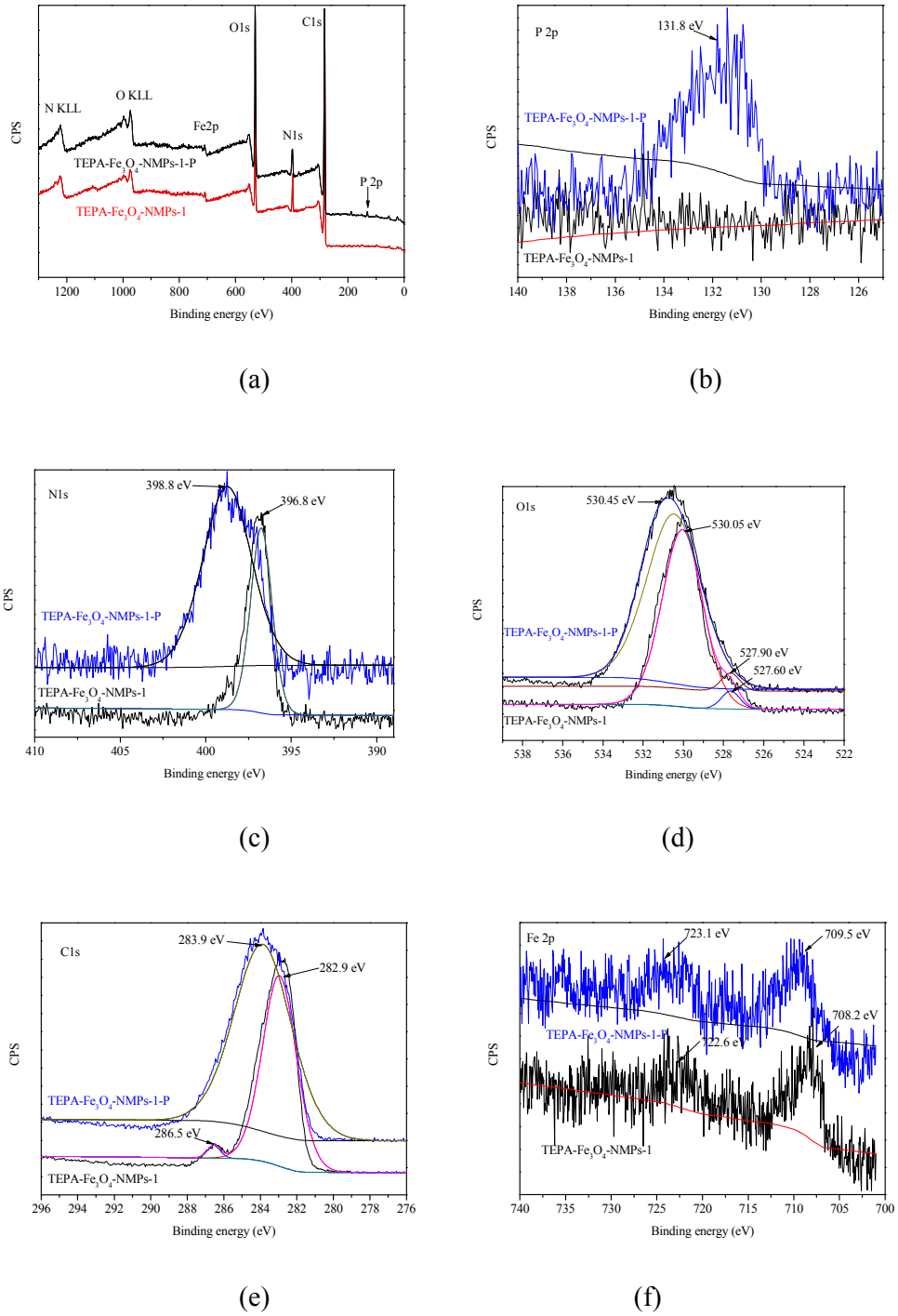

Fig. 3 XPS spectra of: (a) survey scan, and high-resolution scan of: (b) P2p; (c) N1s; (d) O1s; (e) C1s; (f) Fe2p

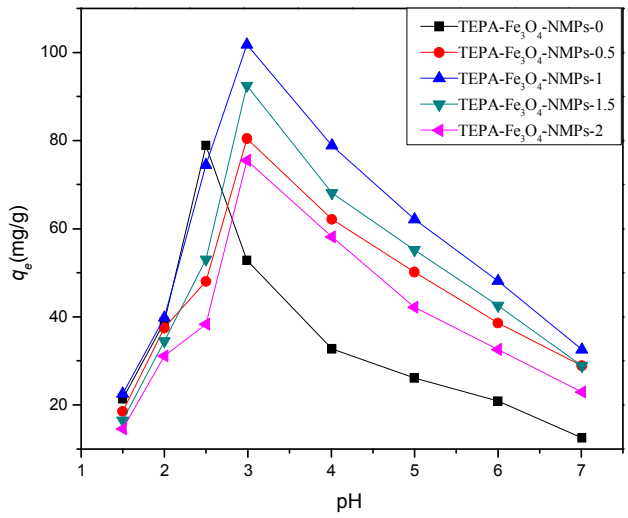

Fig. 4 Effect of pH on the removal of phosphate by different adsorbents

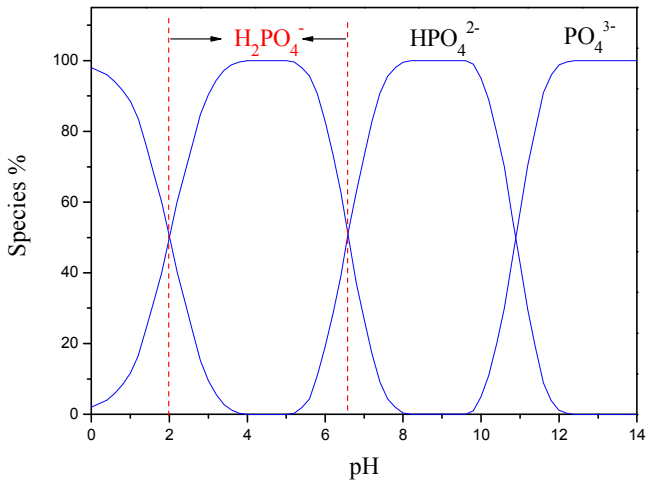

Fig. 5 Distribution diagrams of phosphate species

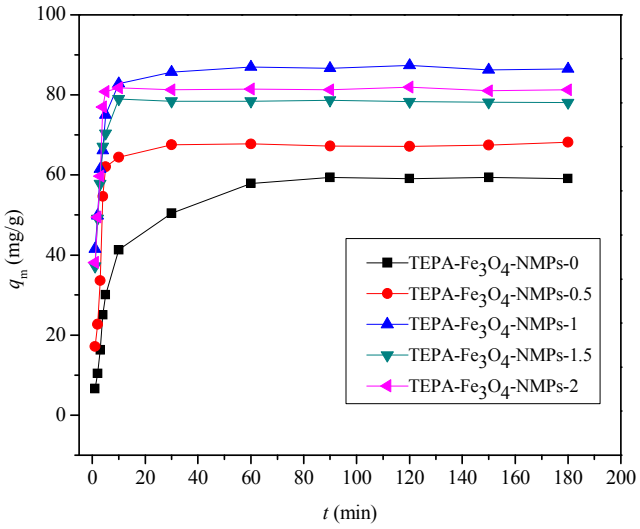

(a)

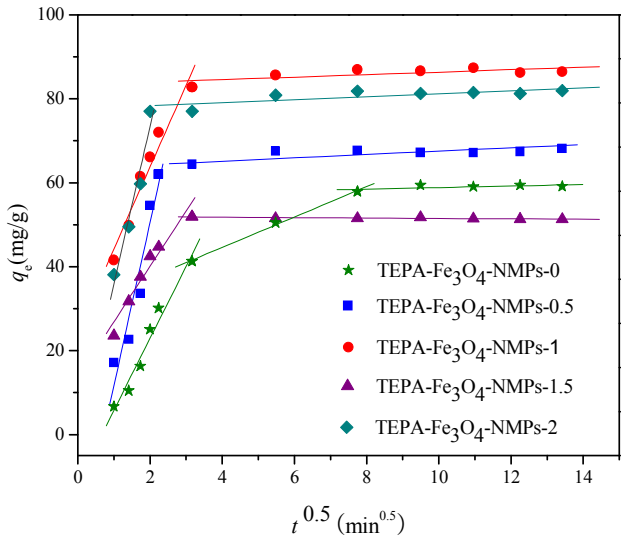

(b)

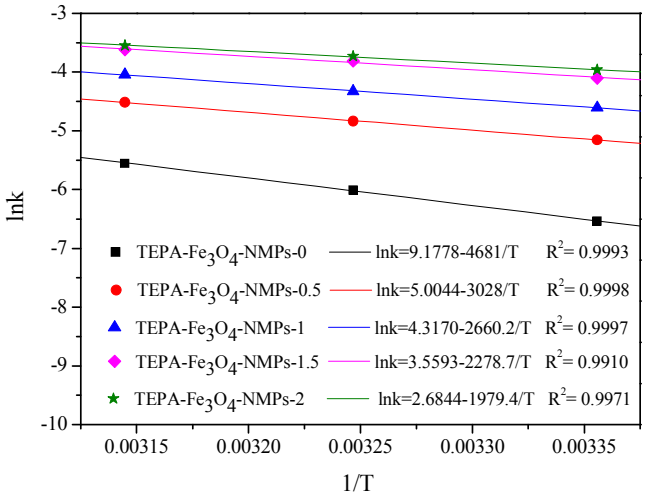

(c)

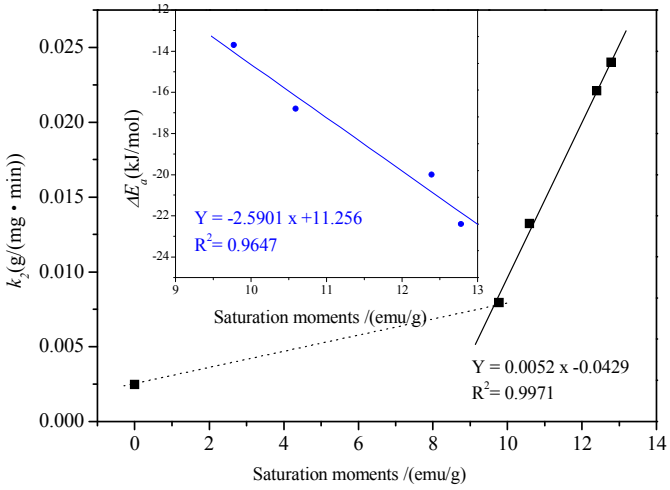

(d)

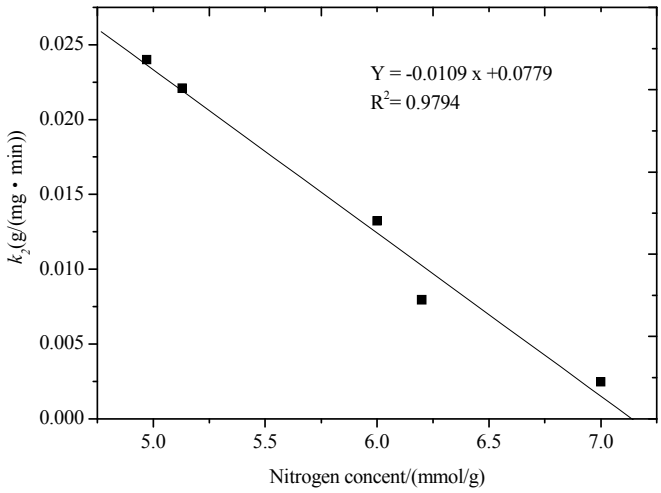

(e)

Fig. 6 Kinetic results for phosphate adsorption: (a) for different adsorbents; (b) Intraparticle diffusion model of phosphate adsorption onto TEPA-Fe_3O_4-NMPs with different usage amounts of magnetic core; (c) plot of ln$k$ *vs* 1/T; (d) Relationship etween k_2 and $\triangle E_a$ (insert) and the saturation moments of the TEPA-Fe_3O_4-NMPs; (e) Relationship between k_2 and the nitrogen contents of the TEPA-Fe_3O_4-NMPs

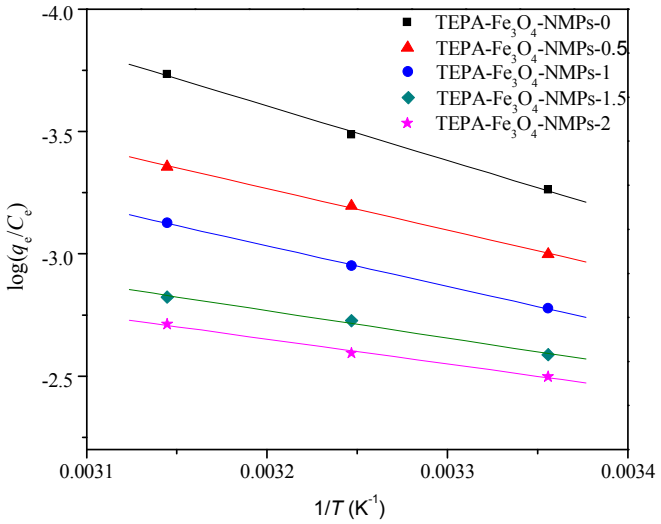

Fig. 7 Thermodynamitic results of adsorption of phosphate onto TEPA-Fe_3O_4-NMPs

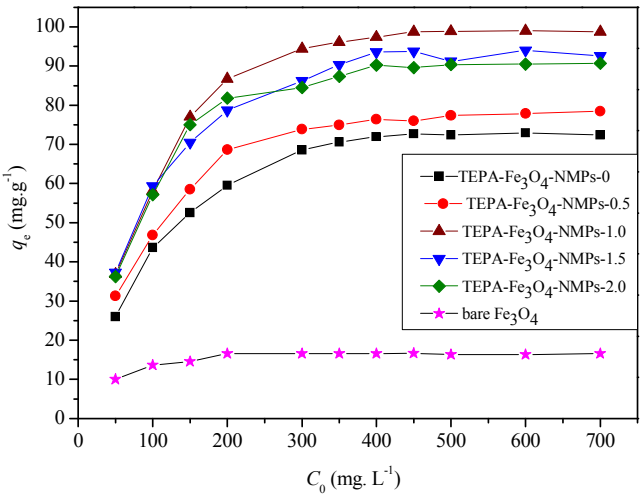

(a)

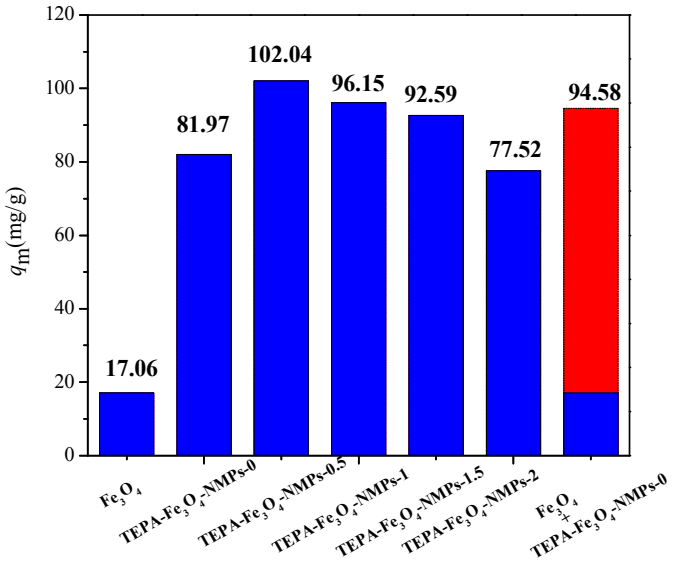

(b)

Fig. 8 Adsorption isotherm of phosphate onto different adsorbents

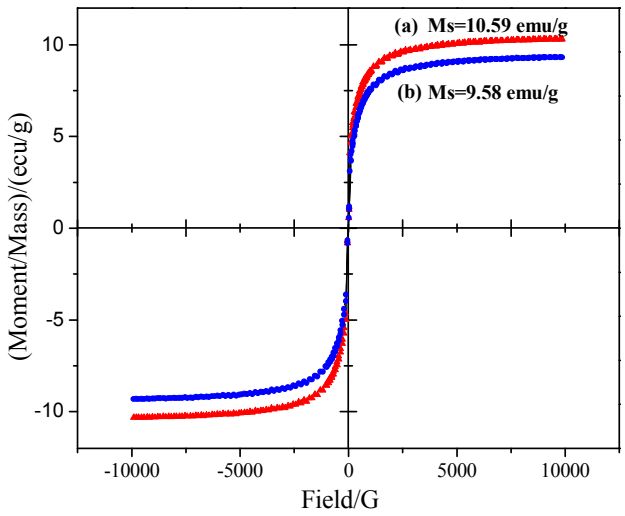

Fig. 9 VSM analysis of: (a) TEPA-Fe_3O_4-NMPs-1; (b) TEPA- Fe_3O_4-NMPs-1-P

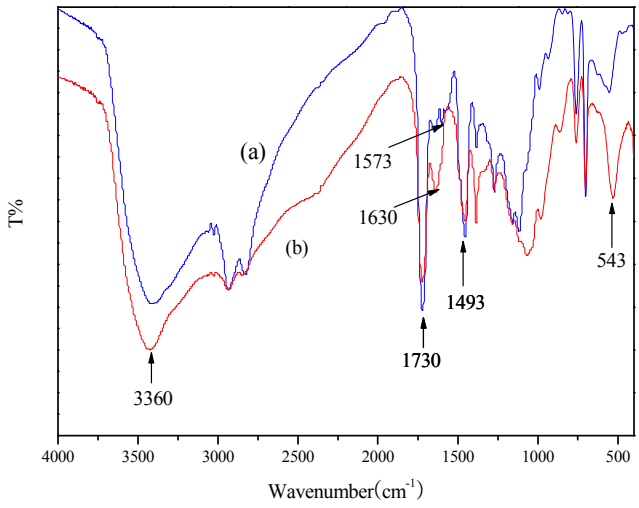

Fig. 10 FTIR analysis of: (a) TEPA- Fe_3O_4-NMPs-1; (b) TEPA-Fe_3O_4-NMPs-1-P

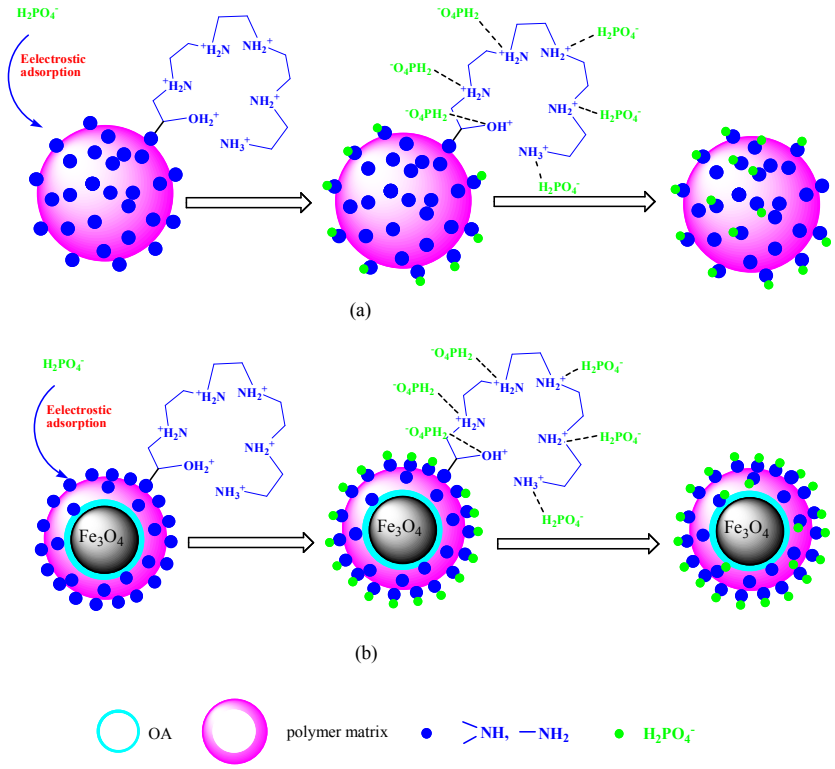

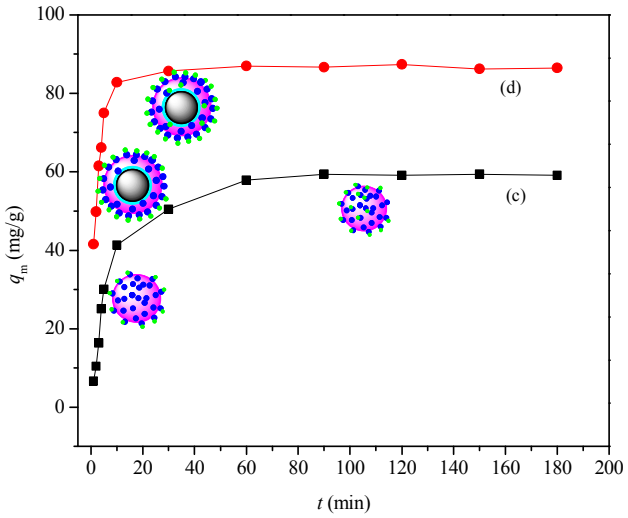

Scheme 1 Presumed adsorption mechanism

Table 1 Content of Fe_3O_4, N and saturation moments of TEPA-Fe_3O_4-NMPs

Adsorbents	Usage amount of Fe_3O_4 (g)	Content of Fe_3O_4 (%)	Content of N ($mmol \cdot g^{-1}$)	Saturation moments ($emu \cdot g^{-1}$)
Bare Fe_3O_4	-	97.53	-	73.98
TEPA-Fe_3O_4-NMPs-0	0	0	5.00	-
TEPA-Fe_3O_4-NMPs 0.5	0.5	13.49	4.43	9.77
TEPA-Fe_3O_4-NMPs -1	1	14.55	4.28	10.59
TEPA-Fe_3O_4-NMPs-1.5	1.5	16.64	3.66	12.39
TEPA-Fe_3O_4-NMPs -2	2	19.24	3.55	12.78

Table 2 Binding energy and atomic concentration of the key elements in TEPA-Fe_3O_4-NMPs

Valence state	Position BE (eV)	TEPA-Fe_3O_4-NMPs -0		TEPA-Fe_3O_4-NMPs-0.5		TEPA-Fe_3O_4-NMPs-1.0		TEPA-Fe_3O_4-NMPs-1.5		TEPA-Fe_3O_4-NMPs-2.0	
		Atomic Concentration (%)		Atomic Concentration (%)		Atomic Concentration (%)		Atomic Concentration (%)		Atomic Concentration (%)	
		before	after	before	after	before	after	before	after	before	after
Fe 2p	709	0	0	0.4	0.42	0.44	0.48	0.5	0.53	0.54	0.58
O 1s	530.5	17.45	21.02	14.53	21.46	15.45	20.59	18.58	25.32	18.05	26.03
N 1s	397.85	4.54	4.42	4.92	4.73	5.88	5.76	7.88	7.16	8.53	8.23
C 1s	284.1	78.01	73.98	80.15	72.63	78.23	72.05	73.04	65.46	72.88	63.4
P 2p	131.25	0	0.58	0	0.76	0	1.12	0	1.53	0	1.76

Table 3 Pseudo-first-order and pseudo-second-order models and constants

Adsorbents	$q_{e,exp}$	Pseudo-first-order model			Pseudo-second-order model		
	(mg/g)	k_1(min^{-1})	$q_{e,cal}$(mg/g)	R^2	k_2(g/(mg·min))	$q_{e,cal}$(mg/g)	R^2
TEPA-Fe_3O_4-NMPs-0	59.09	0.1202	45.51	0.9691	0.00247	61.34	0.9991
TEPA-Fe_3O_4-NMPs-0.5	68.17	0.6771	62.66	0.8297	0.00795	68.49	0.9996
TEPA-Fe_3O_4-NMPs-1	86.46	0.6241	58.35	0.9716	0.0132	86.96	0.9999
TEPA-Fe_3O_4-NMPs-1.5	78.06	0.9382	65.71	0.99	0.0221	78.74	0.9999
TEPA-Fe_3O_4-NMPs-2	81.26	2.0986	174.32	0.9021	0.0241	81.97	0.9999

Table 4 Thermodynamic parameters for adsorption of phosphate onto TEPA-Fe_3O_4-NMPs

Adsorbents	Initial concentration ($mg \cdot L^{-1}$)	ΔH ($kJ \cdot mol^{-1}$)	ΔS ($J \cdot mol^{-1} \cdot K^{-1}$)	ΔG($kJ \cdot mol^{-1}$) /308 K
TEPA-Fe_3O_4-NMPs-0	50	13.55	47.28	-1.02
TEPA-Fe_3O_4-NMPs-0.5	50	11.33	45.54	-2.70
TEPA-Fe_3O_4-NMPs-1	50	7.26	42.19	-5.74
TEPA-Fe_3O_4-NMPs-1.5	50	6.38	40.63	-6.13
TEPA-Fe_3O_4-NMPs-2	50	5.15	33.71	-5.23

Table 5 Langmuir and Freundlich isotherms and constants of phosphate adsorption

Adsorbents	Langmuir isotherm			Freundlich isotherm		
	K_L($L \cdot mg^{-1}$)	q_m($mg \cdot g^{-1}$)	R^2	K_F	$1/n$	R^2
TEPA-Fe_3O_4-NMPs-0	0.0304	77.52	0.9988	14.12	0.2775	0.9050
TEPA-Fe_3O_4-NMPs-0.5	0.0409	81.97	0.9996	20.24	0.2284	0.9262
TEPA-Fe_3O_4-NMPs-1	0.0523	102.04	0.9996	30.93	0.2011	0.9329
TEPA-Fe_3O_4-NMPs-1.5	0.0654	96.15	0.9988	31.93	0.1825	0.9647
TEPA-Fe_3O_4-NMPs-2	0.0747	92.59	0.9996	30.66	0.1866	0.9135
bare Fe_3O_4	0.0609	17.06	0.9987	6.598	0.8194	0.7710